Journal of Materials Chemistry A

ROYAL SOCIETY OF CHEMISTRY

PAPER

View Article Online
View Journal | View Issue

Cite this: J. Mater. Chem. A, 2023, 11, 17821

A metal–organic framework based propylene nano-trap with dual functionalities for highly efficient propylene/propane separation†

Hui-Min Wen, [a] Miaoyu Liu,[a] Yujia Ling,[a] Xiao-Wen Gu,[b] Di Liu,[b] Chenyi Yu,[a] Yulan Liang,[a] Bo Xie, [a] Bin Li *[b] and Jun Hu *[a]

Propylene/propane (C_3H_6/C_3H_8) separation represents one of the most challenging and energy-intensive processes in the petrochemical industry due to their very similar sizes and physical properties. Most of the reported physisorbents still face the challenge of achieving simultaneously high C_3H_6 uptake and selectivity with moderate adsorption enthalpy. Herein, we realize an efficient propylene nano-trap in a microporous MOF (ZJUT-2, $Ni(pyz\text{-}SH)_2SiF_6$) for highly efficient C_3H_6/C_3H_8 separation. This MOF-based propylene nano-trap features a suitable pore cavity decorated with dual functionalities (–SH and SiF_6^{2-}) to optimally interact with the C_3H_6 molecule, affording both large C_3H_6 capture capacity (123.5 cm^3 cm^{-3} at 296 K and 0.5 bar) and high C_3H_6/C_3H_8 selectivity of 17.2 achieved with moderate C_3H_6 adsorption enthalpy (45 kJ mol^{-1}). Theoretical calculations revealed that the appropriate pore cavity and dual functionalities synergistically construct an efficient nano-trap to match better with the C_3H_6 molecule and thus provide stronger multipoint interactions with C_3H_6 over C_3H_8. Actual breakthrough experiments demonstrated that this material can efficiently capture C_3H_6 from C_3H_6/C_3H_8 mixtures (50/50 and 10/90, v/v) under ambient conditions, affording both top-tier C_3H_6 capture amount (2.6 mmol g^{-1}) and dynamic selectivity of 10.

Received 8th May 2023
Accepted 31st July 2023

DOI: 10.1039/d3ta02737f

rsc.li/materials-a

Introduction

Propylene (C_3H_6) is one of the most critical chemical intermediates and an essential raw material used in the production of polypropylene, acrylonitrile, isopropanol, and propylene oxide.[1] In 2018, the global production of polypropylene, as the second most important synthetic plastic (second to polyethylene), was estimated at 56 Mt and will continuously increase to 88 Mt by 2026.[2] For most end uses, the propylene must have a purity of at least 99.5% (polymer-grade).[3] In industry, propylene is typically obtained by steam cracking of naphtha or during fluid catalytic cracking of gas oils in refineries, which involves propane (C_3H_8) as a coproduct.[4] The production of polymer-grade C_3H_6 involves the separation of C_3H_6 from a C_3H_6/C_3H_8 mixture. A conventional method for this separation mainly relies on cryogenic distillation, executed at about 243 K and 0.3 MPa in a column containing over 100 trays.[5] Evidently, such a heat-driven separation process is highly energy-intensive. It is highly demanded to develop alternative and energy-efficient separation technologies to potentially supersede traditional methods.[6]

Non-thermally driven processes, such as adsorptive separation by porous materials, have been considered to dramatically reduce the cost and energy required to purify olefins. In this regard, microporous metal–organic frameworks (MOFs) have been demonstrated to be promising adsorbents for gas separation and purification owing to their tunable pore size/shape and surface functionality.[7–11] Amongst various gas separations, C_3H_6/C_3H_8 separation represents one of the highest separation difficulties due to the subtle molecular size difference between the two components (<0.4 Å). A number of MOFs have been developed in recent years to show high C_3H_6/C_3H_8 separation performance based on equilibrium-based, kinetic-based, molecular sieving or gating-opening mechanisms.[12–30] Nevertheless, there commonly exists a trade-off challenge between uptake capacity and separation selectivity for most of the materials. For instance, several size-selective adsorbents with well-matched pore sizes (*e.g.*, KAUST-7 and Co-gallate) enable complete size-exclusion of C_3H_8 from C_3H_6 to show record C_3H_6/C_3H_8 selectivities but are commonly impaired by their relatively low gas uptakes.[16,18] In contrast, those large-pore MOFs (*e.g.*, HKUST-1 and FeMIL-100) show high C_3H_6 uptakes over 120 cm^3 g^{-1}; however, large pores cannot efficiently discriminate the two similar molecules, resulting in low

[a]College of Chemical Engineering, Zhejiang University of Technology, Hangzhou, Zhejiang 310014, China. E-mail: hjzjut@zjut.edu.cn

[b]State Key Laboratory of Silicon and Advanced Semiconductor Materials, School of Materials Science and Engineering, Zhejiang University, Hangzhou 310027, China. E-mail: bin.li@zju.edu.cn

† Electronic supplementary information (ESI) available: Stability tests, PXRD patterns, adsorption isotherms and breakthrough curves. See DOI: https://doi.org/10.1039/d3ta02737f

selectivity below 5.[29] To overcome this trade-off dilemma, some specific MOFs with gating-opening or thermodynamic–kinetic effects have been realized for benchmark separation properties, while such kinds of materials are difficult to universally design in most cases.[12–19] Another more popular strategy is to immobilize strong open metal sites (OMSs) into MOFs for boosting preferential binding of C_3H_6 over C_3H_8.[25–29] For example, the incorporation of high-density OMSs in MOF-74 or Ag(I) centers in MIL-101-SO_3H can improve C_3H_6/C_3H_8 selectivity up to *ca.* 40 while maintaining a high C_3H_6 adsorption amount.[25–28] However, such high selectivities arise from ultra-strong metal–olefin interactions that are commonly greater than 60 kJ mol^{-1}, leading to high regeneration energy. Evidently, there is a high demand to immobilize suitable functional sites with moderate binding affinity to boost C_3H_6/C_3H_8 selectivity while maintaining high adsorption amounts.

Recent studies have shown that SIFSIX materials (SIFSIX = hexafluorosilicate (SiF_6^{2-})) are very promising adsorbents for hydrocarbon separations because their pore size can be finely tuned and SiF_6^{2-} anions have moderately strong interactions with hydrocarbon molecules.[23,31] For example, two SIFSIX materials (GeFSIX-2-Cu-i and SIFSIX-2-Cu-i) with pore sizes of 4.5–4.7 Å exhibit the selective separation of C_3H_6 over C_3H_8, while the relatively large pore sizes lead to the insufficient selectivity of below 5.[23b] Optimizing the pore size to 3.5 Å in NbOFFIVE-1-Ni can afford full molecular sieving toward C_3H_6/C_3H_8 separation; however, the extremely small pore spaces severely delimit its C_3H_6 uptake.[16] Therefore, simple control of pore sizes with single functionality in SIFSIX materials cannot fully address the trade-off dilemma to target both high C_3H_6 adsorption and selectivity. Herein, we realized the immobilization of dual functionalities in a SIFSIX material (ZJUT-2, $Ni(pyz\text{-}SH)_2SiF_6$, pyz-SH = 2-mercaptopyrazine),[34] to construct an efficient C_3H_6 nano-trap for highly efficient C_3H_6/C_3H_8 separation. This MOF-based nano-trap features not only a small pore cavity with a suitable size of 3.9 × 3.9 × 7.5 $Å^3$ that matches better with a kinetic diameter of C_3H_6 (4.0 Å) than C_3H_8 (4.3 Å),[12,18] but also is decorated with dual functionalities (–SH and SiF_6^{2-}) to optimally interact with the C_3H_6 molecule. This material thus exhibits both top-tier C_3H_6 capture capacity (123.5 $cm^3\ cm^{-3}$ at 0.5 bar and 296 K) and C_3H_6/C_3H_8 selectivity of 17.2 under ambient conditions, achieved by a moderate C_3H_6 heat of adsorption (45 kJ mol^{-1}). The C_3H_6 uptake and selectivity of ZJUT-2a are obviously higher than those of the pristine SIFSIX-3-Ni (76.6 $cm^3\ cm^{-3}$ and 6.6) and most of the top-performing materials reported. Highly efficient separation of C_3H_6 from both 50/50 and 10/90 C_3H_6/C_3H_8 mixtures was confirmed by experimental breakthrough tests, providing both large C_3H_6 uptake (2.6 mmol g^{-1}) and high dynamic selectivity (10). Both values outperform or are comparable to those of some promising MOFs, such as Y-abtc (1.26 mmol g^{-1} and 8.3),[17] KAUST-7 (1.16 mmol g^{-1} and 12),[16] and Ni-NP (2.3 mmol g^{-1} and 9.6).[22a]

Results and discussion

The powder sample of ZJUT-2 was prepared by the reaction of $NiSiF_6$ and pyz-SH in methanol solution at 85 °C according to the previously reported literature.[34] The phase purity and crystallinity of bulk ZJUT-2 were confirmed by powder X-ray diffraction (PXRD), which matched well with that of the simulated patterns (Fig. S1, ESI†). As shown in Fig. 1a, detailed structure analysis revealed that this material consists of two-dimensional (2D) nets based on pyz-SH linkers and metal nodes, which are further pillared by SiF_6^{2-} anions to form the resulting 3D network. Each pore channel is separated by four SiF_6^{2-} anions to form cylindrical nanocages with a size of 3.9 × 3.9 × 7.5 $Å^3$. From a kinetics point of view, the nanocage aperture of 3.9 Å matches better with the kinetic diameter of C_3H_6 (4.0 Å) than C_3H_8 (4.3 Å), making it an ideal single-molecule trap for the capture of single C_3H_6 molecules (Fig. 1b). Most importantly, the incorporated dual functionalities of –SH and SiF_6^{2-} groups are located around the pore channels, which can create a multi-binding nano-trap to optimize the adsorption and recognition of C_3H_6 molecules. Thus, the optimized nano-trap with a suitable size and dual functionalities may provide a single-molecule trap for highly selective capture of C_3H_6 over C_3H_8.

The permanent porosity of ZJUT-2a was first confirmed using the CO_2 adsorption isotherms at 196 K (Fig. S2, ESI†), affording a Brunauer–Emmett–Teller (BET) surface area of 387.8 $m^2\ g^{-1}$. Single component gas adsorption isotherms of C_3H_6 and C_3H_8 for ZJUT-2a were collected at 296 K and 273 K up to 1 bar (Fig. 2a, S3 and S4, ESI†) and compared with those of pristine SIFSIX-3-Ni (Fig. S6, ESI†). As illustrated in Fig. 2a, ZJUT-2a exhibits a steep and high C_3H_6 uptake at 296 K, which is larger than that of C_3H_8 in the whole pressure region. Even at a low pressure of 0.1 bar, ZJUT-2a shows a very high C_3H_6 uptake of 72.3 $cm^3\ cm^{-3}$, which is the highest among the reported MOFs relevant for C_3H_6/C_3H_8 separation except for the MOF-74 series (Fig. 2b).[25–27] In comparison, the C_3H_8 uptake at 0.1 bar (11.9 $cm^3\ cm^{-3}$) is very low, affording a notably high C_3H_6/C_3H_8 uptake ratio of 6.1 at 0.1 bar. Such high low-pressure C_3H_6 uptake indicates that this MOF-based nano-trap can provide a stronger binding affinity with C_3H_6 over C_3H_8, probably attributed to the suitable cage size and dual functionalities that match better with the size and shape of the C_3H_6 molecule. When the pressure increases to 0.5 bar, the C_3H_6 uptake amount can be improved to 123.5 $cm^3\ cm^{-3}$, which is higher than that of most relevant MOFs except for the MOF-74 series.[25–27] It is worth noting that this uptake is superior to that of SIFSIX-3-Ni (76.6 $cm^3\ cm^{-3}$) and most of the current best-performing materials reported (Fig. 2c), such as HIAM-301 (87.0 $cm^3\ cm^{-3}$),[13] UTSA-400 (85.5 $cm^3\ cm^{-3}$),[14] MFM-520 (74.6 $cm^3\ cm^{-3}$),[20] JNU-3a (69.3 $cm^3\ cm^{-3}$),[12] and KAUST-7 (46.0 $cm^3\ cm^{-3}$).[16] At 1 bar and 296 K, the C_3H_6 uptake of ZJUT-2a can further increase to 138.9 $cm^3\ cm^{-3}$. These adsorption behaviors can be supported by the experimental isosteric heat of adsorption (Q_{st}), wherein the initial Q_{st} value of C_3H_6 for ZJU-2a (45 kJ mol^{-1}) is higher than that of C_3H_8 (Fig. S9, ESI†). Further, as shown in Fig. S11 (ESI†), the initial Q_{st} value of ZJUT-2 for C_3H_6 is much higher than that of SIFSIX-3-Ni (38.7 kJ mol^{-1}), indicating that the immobilization of –SH groups can strengthen the C_3H_6 binding affinity. As shown in Fig. 2d, due to the lack of strong OMSs, the Q_{st} value of ZJUT-2a

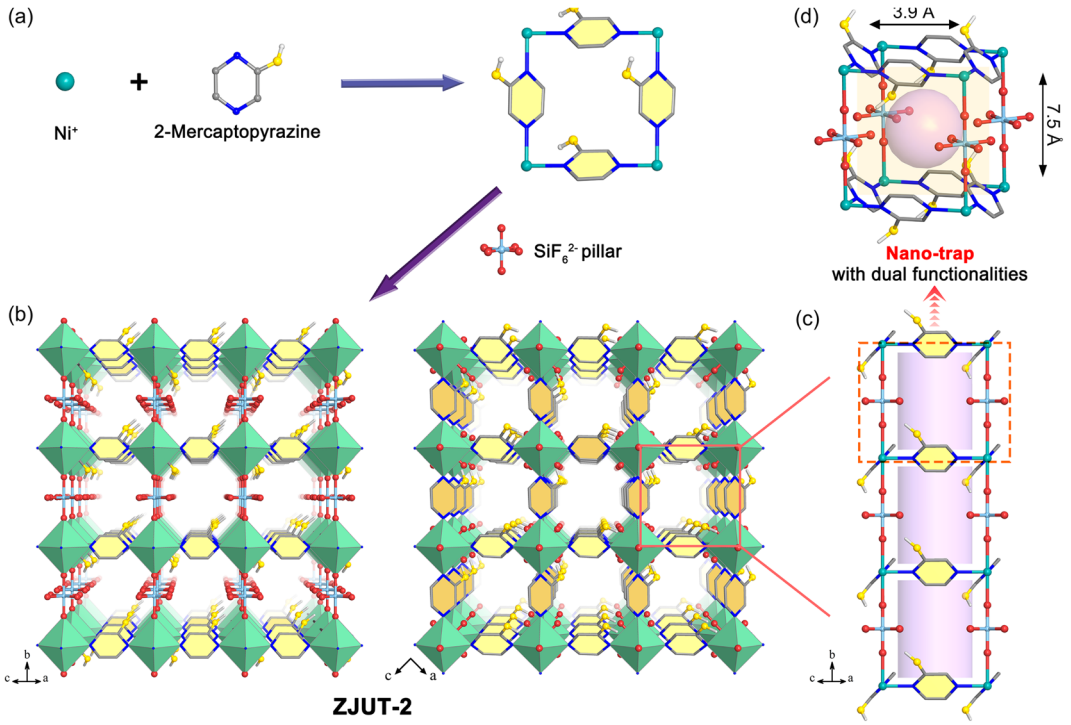

Fig. 1 Structure description of ZJUT-2. (a) Illustration of the square-shaped arrangement in the Ni–pyrazine (4,4′) square grid that is further pillared by anion SiF_6^{2-} blocks to generate a 3D framework. (b) The pore channel structures of ZJUT-2, viewed along the *a*/*c*-axes and the *b*-axis, respectively. (c) The nanocages of ZJUT-2 that are separated by four SiF_6^{2-} anions along the *b*-axis. (d) View of the nano-trap with a size of 3.9 × 3.9 × 7.5 Å^3, decorated with dual functionalities (–SH and SiF_6^{2-}). Color code: F, red; Si, cyan; C, gray; H, white, N, blue; Ni, green; S, yellow.

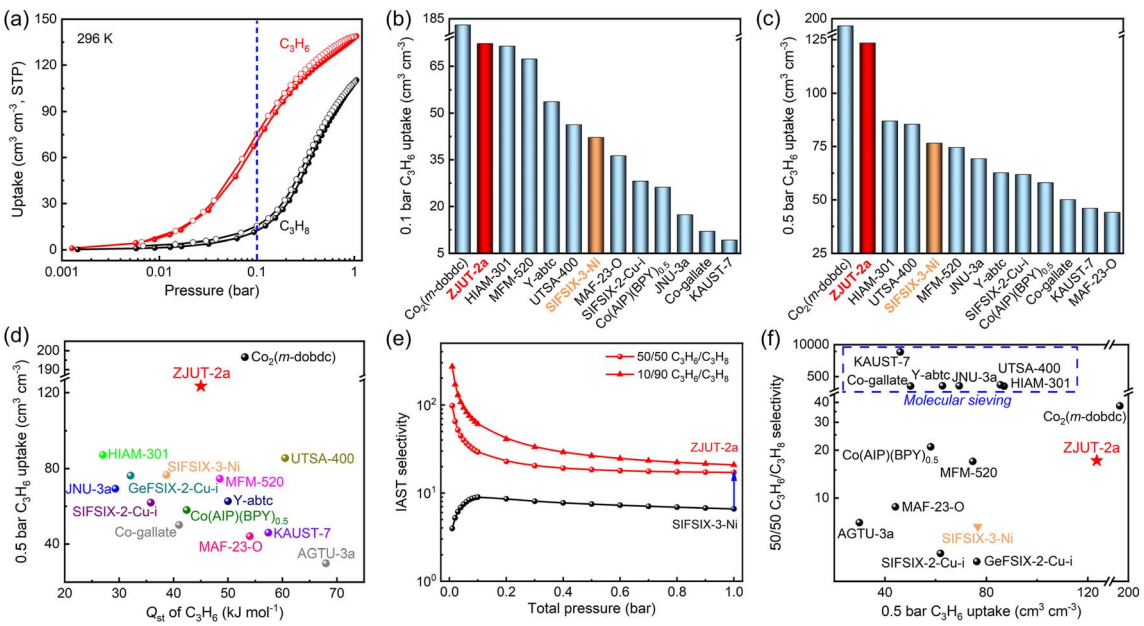

Fig. 2 (a) Adsorption isotherms of C_3H_6 (red) and C_3H_8 (black) for ZJUT-2a at 296 K. (b) Comparison of C_3H_6 uptake capacity for ZJUT-2a and other best-performing materials at 0.1 bar and room temperature. (c) The absorption of C_3H_6 at 0.5 bar and room temperature for ZJUT-2a compared to the indicated best-performing materials. (d) Comparison of heats of adsorption (Q_{st}) of C_3H_6 and C_3H_6 uptake at 0.5 bar and room temperature for ZJUT-2a and other reported materials. (e) The IAST selectivity of 50/50 and 10/90 C_3H_6/C_3H_8 mixtures at 296 K. (f) Comparison of the C_3H_6 uptake capacity at 0.5 bar and C_3H_6/C_3H_8 selectivity for ZJUT-2a and other top-performing adsorbents reported.

is much less than that of the MOF-74 series with high-density OMSs (55–70 kJ mol^{-1}).[25] Therefore, ZJUT-2a exhibits a remarkably top-tier C_3H_6 uptake achieved by a moderate Q_{st} value, compared with all the indicated MOFs as evidenced in Fig. 2d and S12 (ESI†).

The adsorption selectivity of ZJUT-2a for 50/50 and 10/90 C_3H_6/C_3H_8 mixtures was calculated by the ideal adsorbed solution theory (IAST) method. As indicated in Fig. 2e, ZJUT-2a shows a high selectivity of up to 17.2 and 20.9 for 50/50 and 10/90 C_3H_6/C_3H_8 mixtures at 1 bar and 296 K, respectively, which are much higher than that of the pristine SIFSIX-3-Ni (6.6) and other SIFSIX materials such as SIFSIX-2-Cu-i (4.5),[23b] GeFSIX-2-Cu-i (4),[23b] and ZU-36-Ni (10.8).[23a] These values also outperform those of some promising MOFs including Ni–Np (10.5),[22b] MAF-23-O (8.8)[19] and MFM-520 (17),[20] but lower than those of molecular-sieving materials. It should be pointed out that this selectivity value is only for the qualitative comparison purpose. Besides gas selectivity, C_3H_6 uptake capacity at partial pressure is also an important criterion to determine the final separation performance. As shown in Fig. 3f, we comprehensively compared C_3H_6 uptake and selectivity of ZJUT-2a with some promising materials. Although those molecular-sieving MOFs exhibit the record-high selectivity due to the small pore sizes, their C_3H_6 uptakes are relatively low. If we set the C_3H_6 uptake and selectivity as concurrent objectives, most of the reported materials suffer from either unsatisfactory selectivity or inadequate uptake capacity. Evidently, ZJUT-2a, Co_2(*m*-dobdc),[25] UTSA-400 (ref. 14) and HIAM-301 (ref. 13) exhibit more balance between adsorption uptake and gas selectivity for C_3H_6/C_3H_8 separation. Thus, both top-tier C_3H_6 uptake capacity (123.5 cm^3 cm^{-3} at 0.5 bar) and selectivity (17.2) along with moderate adsorption heat make this material among the best-performing materials reported for this separation.

To gain better insight into both high C_3H_6 uptake and selectivity of ZJUT-2, grand canonical Monte Carlo (GCMC) simulations were performed to study the sorbate–sorbent interactions between the framework and gas molecules. The optimal adsorption sites for C_3H_6 and C_3H_8 in the pores of ZJUT-2a are approximated as shown in Fig. 3. Since the cavity size in ZJUT-2a matches well with the C_3H_6 molecule, each nano-trap can only capture one C_3H_6 molecule through multiple hydrogen bonding and van der Waals (vdW) interactions between dual functionalities (–SH and SiF_6^{2-}) and the C_3H_6 molecule. As shown in Fig. 3a and b, each C_3H_6 molecule interacts with four SiF_6^{2-} anions through eleven C–H···F hydrogen bonds with the distances of 2.33–3.09 Å and also binds with four –SH groups through six C–H···S interactions (2.73–3.27 Å). Evidently, the immobilized SiF_6^{2-} and –SH groups synergistically contribute to enforcing the interactions with the C_3H_6 molecule. Further, the dense distribution of these nano-traps within the framework enables the C_3H_6 molecules to be in close proximity to each other with a contact distance of 4.16 Å along the *b* axis (Fig. 3c). Such observed contact distances in ZJUT-2a are notably shorter than those found in JNU-3a (4.53 Å), HIAM-301 (6.03 Å) and also comparable to the C_3H_6···C_3H_6 average distance in the crystalline C_3H_6 (4.47 Å) collected at 65 K.[15,32] This reveals that ZJUT-2a shows the dense packing of C_3H_6 molecules within the pores, thus resulting in its high C_3H_6 uptake capacity. In comparison, the overall H-bonding interactions between the pore surface and C_3H_8 molecule are much less than that of C_3H_6 (Fig. S14 and S15, ESI†). In addition, the cavity sizes of this nano-trap were found to be smaller than the kinetic diameter of C_3H_8. The weaker binding affinity and poor size match with the nano-trap may lead to partially populating the binding sites for C_3H_8. The above reasons thus afford both high C_3H_6 uptake capacity and selectivity.

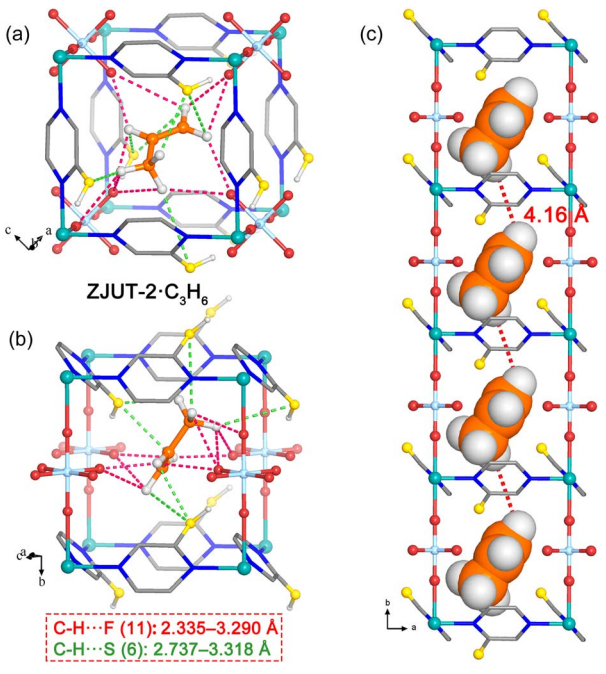

Fig. 3 Illustration of (a) and (b) C_3H_6 adsorption sites in the nano-trap of ZJUT-2a, revealed by theoretical calculations. (c) Dense packing of the adsorbed C_3H_6 molecules within the pore channel of ZJUT-2a, viewed along the *c* axis. Color code: F (red), Si (cyan), C (grey in ZJUT-2, orange in C_3H_6), H (white), N (blue), Ni (green), S (yellow).

To evaluate the actual separation performance of ZJUT-2a, dynamic breakthrough experiments on binary C_3H_6/C_3H_8 gas mixtures were carried out under ambient conditions. As presented in Fig. 4a, ZJUT-2a exhibited a clear separation for the 50/50 C_3H_6/C_3H_8 mixture, wherein pure C_3H_8 first eluted through the adsorption bed at 33 min, while C_3H_6 was retained for a longer time of 65 min. During this breakthrough interval, the C_3H_6 dynamic uptake was calculated to be 2.6 mmol g^{-1}, which is 79% of the saturated uptake (3.3 mmol g^{-1}) obtained from single-component adsorption isotherms at 296 K and 1 bar. This value is not only much higher than that of other reported SIFSIX materials (Fig. 4b), including SIFSIX-3-Ni (1.25 mmol g^{-1}),[23a] GeFSIX-2-Cu-i (2.2 mmol g^{-1}),[23b] and SIFSIX-2-Cu-i (2.0 mmol g^{-1}),[23b] but also outperforms some top-performing MOFs such as JNU-3a (2.45 mmol g^{-1}),[12] HIAM-301 (2.07 mmol g^{-1})[13] and KAUST-7 (1.16 mmol g^{-1}).[16] Further, the dynamic C_3H_6/C_3H_8 selectivity was estimated to be up to 10, which exceeds that of SIFSIX-3-Ni (2.3)[23a] and most top-performing materials, such as Y-abtc (8.3),[17] Co-MOF-74 (6.5)[25] and Ni-NP (9.6).[22a] As shown in Fig. 4c, ZJUT-2a thus shows

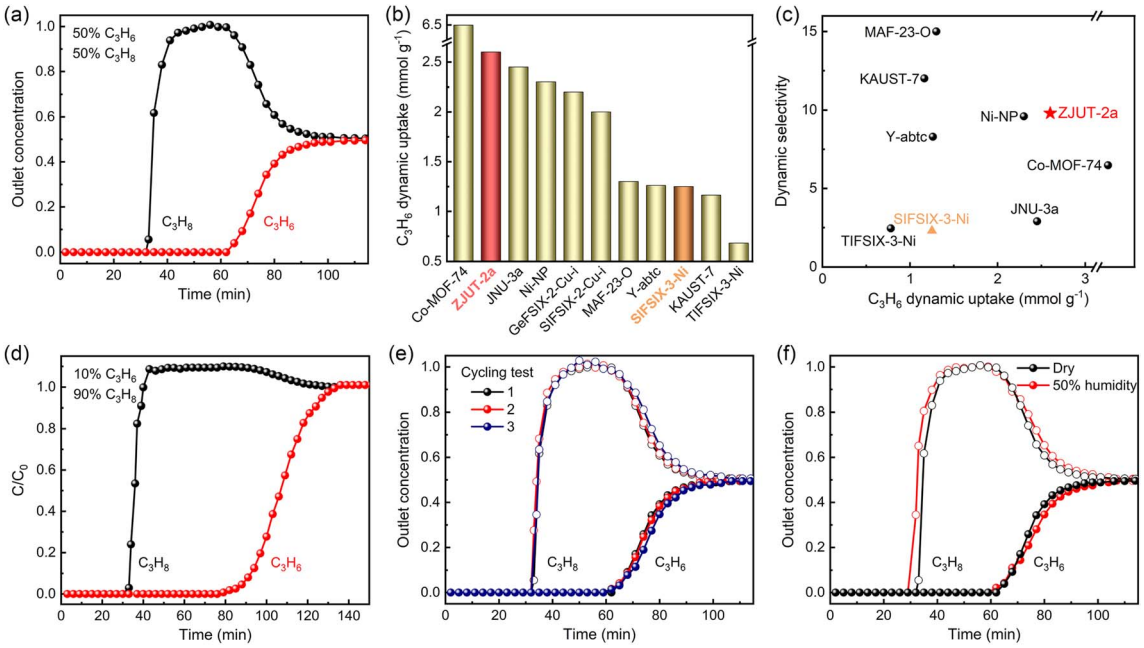

Fig. 4 (a) Experimental breakthrough curves for a 50/50 C_3H_6/C_3H_8 mixture with a flow rate of 2 mL min^{-1} under ambient conditions. (b) Comparison of C_3H_6 dynamic uptake for ZJUT-2a and other benchmark materials. (c) Comparison of C_3H_6 dynamic uptake and selectivity for ZJUT-2a and other benchmark materials. (d) Experimental breakthrough curves for a 10/90 C_3H_6/C_3H_8 mixture with a flow rate of 2 mL min^{-1} under ambient conditions. (e) Cycling column breakthrough curves for 50/50 C_3H_6/C_3H_8 separation under ambient conditions. (f) Breakthrough curves of ZJUT-2a for 50/50 C_3H_6/C_3H_8 separation at 50% humidity.

a rare combination of simultaneously high C_3H_6 dynamic uptake and selectivity, placing it among the best-performing materials reported so far for C_3H_6/C_3H_8 separation. It should be noted that the feed gases in some production processes might contain only a small amount of C_3H_6, which requires adsorbents to efficiently capture C_3H_6 at low partial pressures. Therefore, we performed the breakthrough experiments for 10/90 C_3H_6/C_3H_8 mixtures (Fig. 4d). More difference in the breakthrough times of C_3H_6 and C_3H_8 was observed, with a high dynamic C_3H_6 uptake of 1.5 mmol g^{-1}, indicating the superior separation ability of ZJUT-2a for some gas mixtures with low C_3H_6 content. Three continuous cycles on 50/50 and 10/90 mixtures showed the full retention of the separation performance and easy recyclability of ZJUT-2a (Fig. 4e and S20, ESI†). Given that water vapor is a ubiquitous component in industrial gas mixtures,[33] we conducted the breakthrough experiments for a wet C_3H_6/C_3H_8 mixture at 50% relative humidity. As shown in Fig. 4f, the almost unchanged breakthrough times of both C_3H_6 and C_3H_8 demonstrated the excellent moisture tolerance properties of ZJUT-2a, which can avoid the deleterious effect of water vapor on C_3H_6/C_3H_8 separation performance. As inferred from the PXRD performed on associated samples (Fig. S22, ESI†), the framework of ZJUT-2a remains stable after multiple breakthrough experiments.

Conclusions

In summary, we have realized the immobilization of dual functionalities into a suitable MOF to construct a single-molecule nano-trap for highly efficient C_3H_6/C_3H_8 separation. The incorporated bifunctional groups (–SH and SiF_6^{2-}) combined with the appropriate cavity size/shape in ZJUT-2a can synergistically create multiple binding environments to densely and selectively trap the C_3H_6 molecule, as revealed by theoretical calculations. This MOF-based nano-trap thus exhibited both top-tier C_3H_6 capture capacity (123.5 cm^3 cm^{-3} at 0.5 bar) and C_3H_6/C_3H_8 selectivity of 17.2 under ambient conditions, achieved by a moderate C_3H_6 adsorption enthalpy (45 kJ mol^{-1}). Breakthrough experiment data revealed both remarkably large C_3H_6 dynamic uptake of 2.6 mmol g^{-1} and high dynamic selectivity of 10 for the separation of actual C_3H_6/C_3H_8 mixtures, surpassing most of the top-performing materials reported to date. This work provides some guidance to design porous materials with multiple soft functionalities to highly boost C_3H_6/C_3H_8 separation performance through moderate gas adsorption enthalpy.

Conflicts of interest

There are no conflicts to declare.

Acknowledgements

This work was supported by the National Natural Science Foundation of China (92163110, U1909214 and 92061126) and the Key Research and Development Program of Zhejiang Province (2021C01182).

Notes and references

1 (*a*) I. Amghizar, L. A. Vandewalle, K. M. Van Geem and G. B. Marin, *Engineering*, 2017, **3**, 171–178; (*b*) C. C. E. Christopher, A. Dutta, S. Farooq and I. A. Karimi, *Ind. Eng. Chem. Res.*, 2017, **56**, 14557–14564.

2 C. Tsioptsias, K. Leontiadis, E. Tzimpilis and I. Tsivintzelis, *J. Plast. Film Sheeting*, 2021, **37**, 283–311.

3 V. F. D. Martins, A. M. Ribeiro, M. G. Plaza, J. C. Santos, J. M. Loureiro, A. F. P. Ferreira and A. E. Rodrigues, *J. Chromatogr. A*, 2015, **1423**, 136–148.

4 T. Ren, M. Patel and K. Blok, *Energy*, 2006, **31**, 425–451.

5 S. U. Rege and R. T. Yang, *Chem. Eng. Sci.*, 2002, **57**, 1139–1149.

6 (*a*) A. Marinas, P. Bruijnincx, J. Ftouni, F. J. Urbano and C. Pinel, *Catal. Today*, 2015, **239**, 31–37; (*b*) D. S. Sholl and R. P. Lively, *Nature*, 2016, **532**, 435–437.

7 (*a*) J.-R. Li, R. J. Kuppler and H.-C. Zhou, *Chem. Soc. Rev.*, 2009, **38**, 1477–1504; (*b*) M. C. Das, Q. Guo, Y. He, J. Kim, C.-G. Zhao, K. Hong, S. Xiang, Z. Zhang, K. M. Thomas, R. Krishna and B. Chen, *J. Am. Chem. Soc.*, 2012, **134**, 8703–8710; (*c*) R.-B. Lin, Z. Zhang and B. Chen, *Acc. Chem. Res.*, 2021, **54**, 3362–3376; (*d*) S. Furukawa, J. Reboul, S. Diring, K. Sumida and S. Kitagawa, *Chem. Soc. Rev.*, 2014, **43**, 5700–5734; (*e*) K. Adil, Y. Belmabkhout, R. S. Pillai, A. Cadiau, P. M. Bhatt, A. H. Assen, G. Maurin and M. Eddaoudi, *Chem. Soc. Rev.*, 2017, **46**, 3402–3430; (*f*) H. Wang, Y. Liu and J. Li, *Adv. Mater.*, 2020, **32**, 2002603; (*g*) Z. Chen, K. O. Kirlikovali, P. Li and O. K. Farha, *Acc. Chem. Res.*, 2022, **55**, 579–591.

8 (*a*) L. Li, R.-B. Lin, R. Krishna, H. Li, S. Xiang, H. Wu, J. Li, W. Zhou and B. Chen, *Science*, 2018, **362**, 443–446; (*b*) W. Fan, S. Yuan, W. Wang, L. Feng, X. Liu, X. Zhang, X. Wang, Z. Kang, F. Dai, D. Yuan, D. Sun and H.-C. Zhou, *J. Am. Chem. Soc.*, 2020, **142**, 8728–8737; (*c*) W. Fan, S. B. Peh, Z. Zhang, H. Yuan, Z. Yang, Y. Wang, K. Chai, D. Sun and D. Zhao, *Angew. Chem., Int. Ed.*, 2021, **60**, 17338–17343; (*d*) Y.-Y. Xue, X.-Y. Bai, J. Zhang, Y. Wang, S.-N. Li, Y.-C. Jiang, M.-C. Hu and Q.-G. Zhai, *Angew. Chem., Int. Ed.*, 2021, **60**, 10122–10128; (*e*) H. Li, C. Liu, C. Chen, Z. Di, D. Yuan, J. Pang, W. Wei, M. Wu and M. Hong, *Angew. Chem., Int. Ed.*, 2021, **60**, 7547–7552; (*f*) Y. Yang, L. Li, R.-B. Lin, Y. Ye, Z. Yao, L. Yang, F. Xiang, S. Chen, Z. Zhang, S. Xiang and B. Chen, *Nat. Chem.*, 2021, **13**, 933–939.

9 (*a*) Z. Di, C. Liu, J. Pang, C. Chen, F. Hu, D. Yuan, M. Wu and M. Hong, *Angew. Chem., Int. Ed.*, 2021, **60**, 10828–10832; (*b*) Y. Ye, S. Xian, H. Cui, K. Tan, L. Gong, B. Liang, T. Pham, H. Pandey, R. Krishna, P. C. Lan, K. A. Forrest, B. Space, T. Thonhauser, J. Li and S. Ma, *J. Am. Chem. Soc.*, 2022, **144**, 1681–1689; (*c*) L. Li, L. Guo, D. H. Olson, S. Xian, Z. Zhang, Q. Yang, K. Wu, Y. Yang, Z. Bao, Q. Ren and J. Li, *Science*, 2022, **377**, 335–339; (*d*) T. He, X.-J. Kong, Z.-X. Bian, Y.-Z. Zhang, G.-R. Si, L.-H. Xie, X.-Q. Wu, H. Huang, Z. Chang, X.-H. Bu, M. J. Zaworotko, Z.-R. Nie and J.-R. Li, *Nat. Mater.*, 2022, **21**, 689–695; (*e*) A. N. Hong, E. Kusumoputro, Y. Wang, H. Yang, Y. Chen, X. Bu and P. Feng, *Angew. Chem., Int. Ed.*, 2022, **61**, e202116064; (*f*) G.-D. Wang, R. Krishna, Y.-Z. Li, W.-J. Shi, L. Hou, Y.-Y. Wang and Z. Zhu, *Angew. Chem., Int. Ed.*, 2022, **61**, e202213015.

10 (*a*) H. Zeng, X.-J. Xie, M. Xie, Y.-L. Huang, D. Luo, T. Wang, Y. Zhao, W. Lu and D. Li, *J. Am. Chem. Soc.*, 2019, **141**, 20390–20396; (*b*) H.-G. Hao, Y.-F. Zhao, D.-M. Chen, J.-M. Yu, K. Tan, S. Ma, Y. Chabal, Z.-M. Zhang, J.-M. Dou, Z.-H. Xiao, G. Day, H.-C. Zhou and T.-B. Lu, *Angew. Chem., Int. Ed.*, 2018, **57**, 16067–16071; (*c*) H. Yang, Y. Wang, R. Krishna, X. Jia, Y. Wang, A. N. Hong, C. Dang, H. E. Castillo, X. Bu and P. Feng, *J. Am. Chem. Soc.*, 2020, **142**, 2222–2227; (*d*) Y. Chai, X. Han, W. Li, S. Liu, S. Yao, C. Wang, W. Shi, I. da-Silva, P. Manuel, Y. Cheng, L. D. Daemen, A. J. Ramirez-Cuesta, C. C. Tang, L. Jiang, S. Yang, N. Guan and L. Li, *Science*, 2020, **368**, 1002–1006; (*e*) Y. Wang, T. Li, L. Li, R.-B. Lin, X. Jia, Z. Chang, H.-M. Wen, X.-M. Chen and J. Li, *Adv. Mater.*, 2023, **35**, 2207955; (*f*) J.-X. Wang, C.-C. Liang, X.-W. Gu, H. Wen, C. Jiang, B. Li, G. Qian and B. Chen, *J. Mater. Chem. A*, 2022, **10**, 17878–17916.

11 (*a*) S. Geng, E. Lin, X. Li, W. Liu, T. Wang, Z. Wang, D. Sensharma, S. Darwish, Y. H. Andaloussi, T. Pham, P. Cheng, M. J. Zaworotko, Y. Chen and Z. Zhang, *J. Am. Chem. Soc.*, 2021, **143**, 8654–8660; (*b*) K.-J. Chen, D. G. Madden, S. Mukherjee, T. Pham, K. A. Forrest, A. Kumar, B. Space, J. Kong, Q.-Y. Zhang and M. J. Zaworotko, *Science*, 2019, **366**, 241–246; (*c*) O. T. Qazvini, R. Babarao, Z.-L. Shi, Y.-B. Zhang and S. G. Telfer, *J. Am. Chem. Soc.*, 2019, **141**, 5014–5020; (*d*) K. Su, W. Wang, S. Du, C. Ji and D. Yuan, *Nat. Commun.*, 2021, **12**, 3703; (*e*) K. Shao, H.-M. Wen, C.-C. Liang, X. Xiao, X.-W. Gu, B. Chen, G. Qian and B. Li, *Angew. Chem., Int. Ed.*, 2022, **61**, e202211523; (*f*) J. Pei, X.-W. Gu, C.-C. Liang, B. Chen, B. Li and G. Qian, *J. Am. Chem. Soc.*, 2022, **144**, 3200–3209; (*g*) S. C. Pal, R. Ahmed, A. K. Manna and M. C. Das, *Inorg. Chem.*, 2022, **61**, 18293–18302.

12 H. Zeng, M. Xie, T. Wang, R.-J. Wei, X.-J. Xie, Y. Zhao, W. Lu and D. Li, *Nature*, 2021, **595**, 542–548.

13 L. Yu, X. Han, H. Wang, S. Ullah, Q. Xia, W. Li, J. Li, I. da Silva, P. Manuel, S. Rudić, Y. Cheng, S. Yang, T. Thonhauser and J. Li, *J. Am. Chem. Soc.*, 2021, **143**, 19300–19305.

14 Y. Xie, Y. Shi, E. M. C. Morales, A. El Karch, B. Wang, H. Arman, K. Tan and B. Chen, *J. Am. Chem. Soc.*, 2023, **145**, 2386–2394.

15 D. Liu, J. Pei, X. Zhang, X.-W. Gu, H.-M. Wen, B. Chen, G. Qian and B. Li, *Angew. Chem., Int. Ed.*, 2023, **62**, e202218590.

16 A. Cadiau, K. Adil, P. M. Bhatt, Y. Belmabkhout and M. Eddaoudi, *Science*, 2016, **353**, 137–140.

17 H. Wang, X. Dong, V. Colombo, Q. Wang, Y. Liu, W. Liu, X.-L. Wang, X.-Y. Huang, D. M. Proserpio, A. Sironi, Y. Han and J. Li, *Adv. Mater.*, 2018, **30**, 1805088.

18 (*a*) P. Krokidas, M. Castier, S. Moncho, E. Brothers and I. G. Economou, *J. Phys. Chem. C*, 2015, **119**, 27028–27037;

(*b*) B. Liang, X. Zhang, Y. Xie, R.-B. Lin, R. Krishna, H. Cui, Z. Li, Y. Shi, H. Wu, W. Zhou and B. Chen, *J. Am. Chem. Soc.*, 2020, **142**, 17795–17801; (*c*) Y. Chen, Y. Yang, Y. Wang, Q. Xiong, J. Yang, S. Xiang, L. Li, J. Li, Z. Zhang and B. Chen, *J. Am. Chem. Soc.*, 2022, **144**, 17033–17040.

19 Y. Wang, N.-Y. Huang, X.-W. Zhang, H. He, R.-K. Huang, Z.-M. Ye, Y. Li, D.-D. Zhou, P.-Q. Liao, X.-M. Chen and J.-P. Zhang, *Angew. Chem., Int. Ed.*, 2019, **58**, 7692–7696.

20 J. Li, X. Han, X. Kang, Y. Chen, S. Xu, G. L. Smith, E. Tillotson, Y. Cheng, L. J. M. Mcpherson, S. J. Teat, S. Rudić, A. J. Ramirez-Cuesta, S. J. Haigh, M. Schröder and S. Yang, *Angew. Chem., Int. Ed.*, 2021, **60**, 15541–15547.

21 X.-W. Zhang, D.-D. Zhou and J.-P. Zhang, *Chem*, 2021, **7**, 1006–1019.

22 (*a*) Y. Xie, Y. Shi, H. Cui, R.-B. Lin and B. Chen, *Small Struct.*, 2022, **3**, 2100125; (*b*) Z. Chang, R.-B. Lin, Y. Ye, C. Duan and B. Chen, *J. Mater. Chem. A*, 2019, **7**, 25567–25572.

23 (*a*) Z. Zhang, Q. Ding, X. Cui, X.-M. Jiang and H. Xing, *ACS Appl. Mater. Interfaces*, 2020, **12**, 40229–40235; (*b*) X. Wang, P. Zhang, Z. Zhang, L. Yang, Q. Ding, X. Cui, J. Wang and H. Xing, *Ind. Eng. Chem. Res.*, 2020, **59**, 3531–3537.

24 H. Wu, Y. Yuan, Y. Chen, F. Xu, D. Lv, Y. Wu, Z. Li and Q. Xia, *AIChE J.*, 2020, **66**, e16858.

25 J. E. Bachman, M. T. Kapelewski, D. A. Reed, M. I. Gonzalez and J. R. Long, *J. Am. Chem. Soc.*, 2017, **139**, 15363–15370.

26 Y.-S. Bae, C. Y. Lee, K. C. Kim, O. K. Farha, P. Nickias, J. T. Hupp, S. T. Nguyen and R. Q. Snurr, *Angew. Chem., Int. Ed.*, 2012, **51**, 1857–1860.

27 E. D. Bloch, W. L. Queen, R. Krishna, J. M. Zadrozny, C. M. Brown and J. R. Long, *Science*, 2012, **335**, 1606–1610.

28 G. Chang, M. Huang, Y. Su, H. Xing, B. Su, Z. Zhang, Q. Yang, Y. Yang, Q. Ren, Z. Bao and B. Chen, *Chem. Commun.*, 2015, **51**, 2859–2862.

29 (*a*) N. Lamia, M. Jorge, M. A. Granato, F. A. A. Paz, H. Chevreau and A. E. Rodrigues, *Chem. Eng. Sci.*, 2009, **64**, 3246–3259; (*b*) S.-Y. Kim, T.-U. Yoon, J. H. Kang, A.-R. Kim, T.-H. Kim, S.-I. Kim, W. Park, K. C. Kim and Y.-S. Bae, *ACS Appl. Mater. Interfaces*, 2018, **10**, 27521–27530; (*c*) J. W. Yoon, A.-R. Kim, M. J. Kim, T.-U. Yoon, J.-H. Kim and Y.-S. Bae, *Microporous Mesoporous Mater.*, 2019, **279**, 271–277.

30 M. H. Mohamed, Y. Yang, L. Li, S. Zhang, J. P. Ruffley, A. G. Jarvi, S. Saxena, G. Veser, J. K. Johnson and N. L. Rosi, *J. Am. Chem. Soc.*, 2019, **141**, 13003–13007.

31 (*a*) P. Nugent, Y. Belmabkhout, S. D. Burd, A. J. Cairns, R. Luebke, K. Forrest, T. Pham, S. Ma, B. Space, L. Wojtas, M. Eddaoudi and M. J. Zaworotko, *Nature*, 2013, **495**, 80–84; (*b*) O. Shekhah, Y. Belmabkhout, Z. Chen, V. Guillerm, A. Cairns, K. Adil and M. Eddaoudi, *Nat. Commun.*, 2014, **5**, 4228; (*c*) X. Cui, K. Chen, H. Xing, Q. Yang, R. Krishna, Z. Bao, H. Wu, W. Zhou, X. Dong, Y. Han, B. Li, Q. Ren, M. J. Zaworotko and B. Chen, *Science*, 2016, **353**, 141–144; (*d*) B. Li, X. Cui, D. O'Nolan, H.-M. Wen, M. Jiang, R. Krishna, H. Wu, R.-B. Lin, Y.-S. Chen, D. Yuan, H. Xing, W. Zhou, Q. Ren, G. Qian, M. J. Zaworotko and B. Chen, *Adv. Mater.*, 2017, **29**, 1704210; (*e*) P. Zhang, Y. Zhong, Y. Zhang, Z. Zhu, Y. Liu, Y. Su, J. Chen, S. Chen, Z. Zeng, H. Xing, S. Deng and J. Wang, *Sci. Adv.*, 2022, **8**, eabn9231; (*f*) Y. Jiang, J. Hu, L. Wang, W. Sun, N. Xu, R. Krishna, S. Duttwyler, X. Cui, H. Xing and Y. Zhang, *Angew. Chem., Int. Ed.*, 2022, **61**, e202200947.

32 R. L. Hudson, P. A. Gerakines, Y. Y. Yarnall and R. T. Coones, *Icarus*, 2021, **354**, 114033.

33 S. M. Sadrameli, *Fuel*, 2016, **173**, 285–297.

34 H.-M. Wen, C. Liao, L. Li, L. Yang, J. Wang, L. Huang, B. Li, B. Chen and J. Hu, *Chem. Commun.*, 2019, **55**, 11354–11357.